



**HAL**  
open science

## Consequences of rapid ice sheet melting on the Sahelian population vulnerability

Dimitri Defrance, Gilles Ramstein, Sylvie Charbit, Mathieu Vrac, Adjoua Moïse Famien, Benjamin Sultan, Didier Swingedouw, Christophe Dumas, François Gemenne, Jorge Alvarez-Solas, et al.

### ► To cite this version:

Dimitri Defrance, Gilles Ramstein, Sylvie Charbit, Mathieu Vrac, Adjoua Moïse Famien, et al.. Consequences of rapid ice sheet melting on the Sahelian population vulnerability. Proceedings of the National Academy of Sciences of the United States of America, 2017, 114 (25), pp.6533-6538. 10.1073/pnas.1619358114 . ird-01534034

**HAL Id: ird-01534034**

**<https://ird.hal.science/ird-01534034>**

Submitted on 7 Jun 2017

**HAL** is a multi-disciplinary open access archive for the deposit and dissemination of scientific research documents, whether they are published or not. The documents may come from teaching and research institutions in France or abroad, or from public or private research centers.

L'archive ouverte pluridisciplinaire **HAL**, est destinée au dépôt et à la diffusion de documents scientifiques de niveau recherche, publiés ou non, émanant des établissements d'enseignement et de recherche français ou étrangers, des laboratoires publics ou privés.

1 *Classification :*  
2 SOCIAL SCIENCES: Sustainability Science  
3 PHYSICAL SCIENCES: Earth, Atmospheric, and Planetary Sciences  
4

## 5 **Consequences of rapid ice-sheet melting on the** 6 **Sahelian population vulnerability** 7

8 *Author Affiliation:*

9 Dimitri Defrance (1,2), Gilles Ramstein (1), Sylvie Charbit (1), Mathieu Vrac (1), Adjoua Moïse  
10 Famien (3,2), Benjamin Sultan (2), Didier Swingedouw (4), Christophe Dumas (1), François  
11 Gemenne (5,6), Jorge Alvarez-Solas (7), and Jean-Paul Vanderlinden (5)  
12

13 (1) LSCE/IPSL, CEA-CNRS-UVSQ, Université Paris-Saclay, Gif-sur-Yvette, France

14 (2) Sorbonne Universités, UPMC - CNRS-IRD-MNHN, LOCEAN/IPSL, Paris, France

15 (3) LAPA, Université Félix Houphouët Boigny, Abidjan, Côte-d'Ivoire

16 (4) EPOC, Université de Bordeaux, Pessac, France

17 (5) CEARC, OVSQ, Université Paris-Saclay, Guyancourt, France

18 (6) The Hugo Observatory, FNRS, University of Liège, Belgium

19 (7) PalMA Group, Universidad Complutense de Madrid, Madrid, Spain  
20

21 *Corresponding Author :*

22 Dimitri Defrance

23 Université Pierre et Marie Curie

24 Boîte 100, 4 place Jussieu

25 75252 Paris Cedex 05

26 France

27 Tel : +33 6 49 49 89 48

28 E-mail : dimitri.defrance@ird.fr  
29

30 *Keywords:*

31 climate change ; ice-sheet melting ; impact ; agriculture ; sahel

32 **Abstract**

33 The acceleration of ice sheet melting has been observed over the last few decades. Recent  
34 observations and modeling studies have suggested that the ice sheet contribution to future  
35 sea level rise could have been underestimated in the latest Intergovernmental Panel on  
36 Climate Change report. The ensuing freshwater discharge coming from ice sheets could have  
37 significant impacts on global climate, and especially on the vulnerable tropical areas. During  
38 the last glacial/deglacial period, megadrought episodes were observed in the Sahel region at  
39 the time of massive iceberg surges, leading to large freshwater discharges. In the future, such  
40 episodes have the potential to induce a drastic destabilization of the Sahelian agroecosystem.  
41 Using a climate modeling approach, we investigate this issue by superimposing on the  
42 Representative Concentration Pathways 8.5 (RCP8.5) baseline experiment a Greenland flash  
43 melting scenario corresponding to an additional sea level rise ranging from 0.5 m to 3 m. Our  
44 model response to freshwater discharge coming from Greenland melting reveals a significant  
45 decrease of the West African monsoon rainfall, leading to changes in agricultural practices.  
46 Combined with a strong population increase, described by different demography projections,  
47 important human migration flows could be potentially induced. We estimate that, without  
48 any adaptation measures, tens to hundreds million people could be forced to leave the Sahel  
49 by the end of this century. On top of this quantification, the sea level rise impact over coastal  
50 areas has to be superimposed, implying that the Sahel population could be strongly at threat  
51 in case of rapid Greenland melting.

52 **Significance Statement**

53 A major uncertainty concerning the 21st century climate is the ice sheet response to global  
54 warming. Paleodata indicate rapid ice sheet destabilizations during the last deglaciation,  
55 which could lead to an underestimation of sea level rise, as suggested in recent publications.  
56 Therefore, we explore the impact of different scenarios of Greenland partial melting in the  
57 very sensitive Sahel region. We first demonstrate that such a melting induces a drastic  
58 decrease of West African monsoon precipitation. Moreover, we quantify the agricultural area  
59 losses due to monsoon changes. Consequently, we pinpoint a large potential for migration of  
60 millions of people in the coming decades. Thus, the ice sheet destabilization provokes not only  
61 coastal damages but also large population migration in monsoon area.

62 The Sahel is particularly exposed to extreme climate variability, as evidenced by the impacts  
63 of the severe droughts in the late 20th century (1). Paleoclimatic records have also shown that  
64 megadrought episodes occurred in this area during past glacial/deglacial periods (2↓↓↓–5) at  
65 the time of huge surges of icebergs (i.e., the so-called Heinrich events), causing outlet glacier  
66 acceleration and thus sea level rise (6, 7) (SLR). Several modeling studies performing water-  
67 hosing experiments confirmed the close correspondence between the West African monsoon  
68 weakening and the freshwater flux (FWF) released to the ocean (8↓↓–10) due to ice sheet  
69 melting. These studies raise the question as to whether such episodes could occur during this  
70 century in response to a massive freshwater discharge triggered by a significant ice sheet  
71 destabilization or surface melting and, if so, what would be the related environmental and  
72 human impacts in the Sahel area.

73

74 According to the latest Intergovernmental Panel on Climate Change Fifth Assessment Report  
75 (AR5) (11), the likely range of global mean SLR under the Representative Concentration  
76 Pathways 8.5 (RCP8.5) scenario is 0.52 m to 0.98 m by the end of the 21st century. Although  
77 considerable progress has been made in ice sheet modeling over the last decade, this range is  
78 provided with only medium confidence, due to large remaining uncertainties in the ice sheet  
79 dynamic response and to an improper representation of the ice–ocean interactions (12).

80

81 In Greenland, recent observations of fjords standing well below sea level suggest important  
82 processes of glacier front destabilization (13) that are not included in the current dynamic ice  
83 sheet models (14). Moreover, although there are only a few ice shelves surrounding  
84 Greenland compared with West Antarctica, post-AR5 remote sensing observations reveal that  
85 ice shelves have experienced a continuous thinning for several years, resulting in a buttressing  
86 weakening (15, 16), not only in the Antarctic ice sheet but also in Greenland. This leads to a  
87 significant ice stream acceleration and possibly to a massive discharge of grounded ice, similar  
88 to what occurred during Heinrich events or, more recently, after the collapse of the Larsen B  
89 ice shelf (17). Moreover, past episodes of rapid SLR acceleration, such as the Meltwater Pulse  
90 1A (18), are still raising questions about our ability to evaluate the future SLR under current  
91 understanding of physical mechanisms.

92

93 Results from these past climate studies combined with present-day observations suggest that  
94 the ice sheet contribution to SLR could have been underestimated. Here, we consider different  
95 freshwater discharge scenarios equivalent to an additional SLR ranging from 0.5 m to 3 m  
96 coming from ice sheet melting and/or destabilization, which is not accounted for in the  
97 baseline RCP8.5 climate simulation. We explore the related climatic effects on the West  
98 African monsoon over the 21st century and their ensuing impacts on the Sahelian cultivable  
99 areas and thus on the local population.

100

101 Using the Institut Pierre Simon Laplace low resolution coupled ocean–atmosphere model  
102 (IPSL-CM5A-LR) [same version as in the Coupled Model Intercomparison Project, Phase 5  
103 (CMIP5) exercise (19); Methods] run under the RCP8.5 radiative forcing from 2006 to 2100,  
104 we performed four different water-hosing experiments superimposed to the RCP8.5 scenario  
105 in which we added, respectively, a 0.11-, 0.22-, 0.34-, and 0.68-Sv FWF (1 Sv =  $10^6 \text{ m}^3\cdot\text{s}^{-1}$ )  
106 released in the North Atlantic from 2020 to 2070 and corresponding, respectively, to 0.5-, 1-,  
107 1.5-, and 3-m SLR. Our goal is, first, to investigate the climatic impacts of the FWF coming from  
108 Greenland (GrIS scenarios) in the West African region and, second, to show the impacts on  
109 the cereal cultivation in the Sahel area, and the consequences for the local population, which  
110 is already facing chronic malnutrition problems.

### 111 **Changes in tropical precipitation systems**

112 It has been shown that the freshening of the North Atlantic has global climatic impacts (9,  
113 20↓↓↓↓–25), including a strong cooling of the Northern Hemisphere down to the Sahara  
114 (26↓↓–29) related to a very strong slowdown of the North Atlantic Deep Water (NADW)  
115 leading to the slowdown of the Atlantic meridional overturning circulation (AMOC) (9, 20↓↓↓–  
116 24). The maximum decrease of the mean annual NADW outflow at 30°N occurs around 2060  
117 and corresponds to a reduction of 90% (60%) of the initial NADW value associated with a sea  
118 level rise of 3 m (0.5 m) (Fig. 1A). This feature is associated with a large decrease of Sahel  
119 rainfall (10% to 60%) between 2030 and 2060 with respect to the RCP8.5 scenario (Fig. 2). This  
120 spatial pattern of precipitation changes is similar to the one inferred from the large surge of  
121 iceberg discharges that occurred in the past (2, 30). The tropical rainfall changes are linked to  
122 the Northern Hemisphere cooling through atmospheric teleconnections. A north–south  
123 thermal gradient between the Sahara (cooler) and the Guinea Gulf (warmer) appears (Fig. 1B).  
124 This gradient leads to a rise of sea level pressure gradient, inducing low-level southward winds,

125 which block the monsoon system farther south (Fig. 1C). The Sahel becomes drier, and the  
126 surface temperature increases; this causes an additional local temperature gradient that  
127 strengthens the African Easterly Jet, causing a moisture export from this area (2, 31) (Fig. 1D).  
128 These mechanisms underlying the drastic reduction of Sahelian precipitation are robust in  
129 different climatic contexts with several models (9, 22).

130 Here we focus on the Western African Sahel region (8°N to 18°N; 17°W to 15°E). Because the  
131 Sahelian population is strongly dependent on pastoralism and rainfed agriculture for  
132 subsistence (32), our analysis is made in terms of summer precipitation changes [June to  
133 September (JJAS)] during which most of the rainfall occurs (between 80% and 90%). To  
134 circumvent the acknowledged difficulties of CMIP5 models (33) to properly capture the  
135 mesoscale processes and therefore the monsoon rainfall, we applied a statistical method to  
136 improve the IPSL simulated precipitation in the West African region with respect to the Water  
137 and Global Change project (WATCH) Forcing Data methodology applied to the latest global  
138 atmospheric reanalysis data produced by the European Centre for Medium-Range Weather  
139 Forecasts (ERA-Interim) (WFDEI) reanalysis (34). This method, called “Cumulative Distribution  
140 Function transform” (CDF-t), has been successfully applied in many climate-related studies  
141 (e.g., refs. 35–38; Methods).

142

143 To illustrate the internal model variability, we considered a four-member dataset of the  
144 RCP8.5 scenario, each member differing in initial conditions. The evolution of the corrected  
145 precipitation in the West African Sahel region, obtained under the RCP8.5 dataset (baseline  
146 experiments) and the four GrIS scenarios, is displayed in Fig. 3. However, the precipitation  
147 signal simulated in response to the 0.5-m SLR perturbation is not statistically significant  
148 compared with the four members of the RCP8.5 baseline experiment, as indicated by the t  
149 test (P value <0.05; Methods), and the corresponding results will not be further discussed in  
150 the following.

151 The effect of the FWF perturbation radically changes the evolution of precipitation averaged  
152 over the Sahel region. The first key feature is a significant decrease of Sahel rainfall for the  
153 three larger GrIS scenarios (i.e., 1-, 1.5-, and 3-m equivalent SLR) compared with the four-  
154 member RCP8.5 dataset. This decrease occurs almost concomitantly with the FWF release and  
155 can be up to 30% over the period 2030–2060, reaching 3 mm·d<sup>-1</sup>, where the greatest  
156 differences with the baseline experiment scenario are simulated (P value <0.05). When the

157 freshwater perturbation stops,  $P_{av}$  increases slightly, and values close to those of the baseline  
158 experiment are recovered.

### 159 **Increasing vulnerability**

160 The Sahelian agroecosystem is likely to be strongly disturbed by these large precipitation  
161 changes; this could have significant impacts on populations extremely dependent upon  
162 rainfed agriculture for subsistence. It is documented that the rainfall decrease and the  
163 temperature elevation in the Sahel will negatively impact yields of staple food cereals, such as  
164 sorghum and millet (39). The water demand for these crops is calculated by Food and  
165 Agriculture Organization (FAO) formulations (Methods) and depends on temperature. The  
166 north–south gradient of water demand has a similar amplitude for sorghum and millet,  
167 directly related to the temperature gradient. In the Sahel area, the sorghum needs, currently,  
168 between 520 mm and 660 mm per growing period. The millet growth period is shorter than  
169 that of sorghum and needs therefore less water (460 mm to 600 mm per growing period). The  
170 water demand increases over the 21st century, due to the temperature increase. In average  
171 on the Sahel area, the water demand values rise from 580 mm (515 mm) to 650 mm (580 mm)  
172 per growing period for the sorghum (millet).

173  
174 To quantify the impacts of rainfall decrease on the population, we analyze the gain or loss of  
175 available area for agriculture relative to the adequacy between the sorghum water  
176 requirement and the JJAS precipitation. Fig. 4A displays the variations of available area for  
177 sorghum cultivation. Under the GrIS scenarios, a strong decrease of the cultivable area with  
178 respect to 1976–2005 is observed between 2025 and 2100, up to  $\sim 1,100,000$  km<sup>2</sup> for the 1-  
179 m GrIS melting scenario and even more for the 1.5- and 3-m GrIS melting scenarios. After  
180 2070, the cultivable area slightly increases, and the RCP8.5 values are progressively recovered,  
181 except for the 3-m scenario.

182  
183 The large impact of the GrIS scenarios on the local population may be enhanced by a strong  
184 demography dynamics in the Sahel. All of the projections of the demography evolution  
185 suggest an increase of the population over Africa (40). However, these projections remain  
186 uncertain and are strongly dependent on socioeconomic changes that will occur throughout  
187 the 21st century (40, 41). To estimate the range of people affected by monsoon variations, we  
188 analyze the human impacts related to a loss of cultivable areas for a demography fixed to that

189 of 2011 (lower bound) and for an evolving demography deduced from a shared socioeconomic  
190 pathway (41) (SSP3 hereafter), which is consistent with the RCP8.5 scenario (upper bound).

191

192 Considering the Sahelian population fixed to its 2011 level (i.e., 135 million people, Fig. 4B),  
193 the GrIS scenarios lead to a rapid growth (in less than 20 y) of people impacted by the loss of  
194 cultivable area, up to ~60 million people in the 1.5- and 3-m GrIS melting scenarios between  
195 2040 and 2065, due to change in precipitation regimes. This number slightly decreases at the  
196 end of the FWF perturbation. However, the most dramatic consequences are observed when  
197 the population dynamics are accounted for (Fig. 4C). According to the SSP3 scenario, the  
198 number of people living below the water threshold (Methods) for sorghum cultivation  
199 undergoes a rapid and continuous increase, up to ~360 million by the end of the 21st century.  
200 This number represents one third of the population living in the Sahel area, showing that the  
201 climatic impact is widely amplified by the demography explosion. This situation will put a  
202 considerable strain on millet and sorghum subsistence agriculture. For local farmers,  
203 migration might thus appear as a necessary option, especially if one considers the rapid  
204 development of African metropolises. Options are, indeed, likely to be limited for local  
205 farmers, and staying on their land would require substantial changes in agricultural techniques  
206 and the abandonment of subsistence agriculture (42).

207

208 We demonstrated that Greenland melting during the 21st century could drastically affect the  
209 climate, not only in high-latitude locations but also over the tropical areas, through  
210 atmospheric and oceanic teleconnections. Although most studies focus on the coastal impacts  
211 of SLR (43), we pointed out that Greenland melting could produce drastic droughts in the  
212 Sahel, with many consequences for agricultural practices and for population migrations. In the  
213 past, monsoon-dependent farmers have used the cities (44) and the coastal zones as a refuge  
214 or a final migration destination following rainfall deficit years. Under the 1-m SLR scenario or  
215 one involving higher SLR, coastal zones will be extremely destabilized, and migration to these  
216 regions will be difficult, with a possible “coastal squeeze” (45), making the urban areas the  
217 primary destination for migrants. Today, most migrant flows related to environmental  
218 disruptions occur within their national or regional boundaries (46). A rapid melting of ice  
219 sheets, however, is likely to lead to dramatic population shifts that would develop beyond  
220 borders and would entail irreversible demographic impacts.



## 221 **Methods**

222

### 223 **Model and experimental details**

224

### 225 **Model and Experimental Details**

226 All of the experiments presented in this study have been carried out with the coupled  
227 atmosphere–ocean IPSL-CM5A-LR model (19), which has been used for the CMIP5 exercise.  
228 The atmospheric component has a spatial resolution of  $3.75^\circ \times 1.875^\circ$  in longitude and  
229 latitude, respectively, with 39 vertical levels; the oceanic component uses an irregular grid  
230 with a nominal resolution of  $2^\circ$ , and a higher latitudinal resolution of  $0.5^\circ$  in the equatorial  
231 ocean, and 31 vertical levels. The locations of freshwater inputs have been designed to  
232 produce a rapid response of the model. We therefore chose to release the freshwater in  
233 locations of deep water formations, in the North Atlantic ( $45^\circ\text{N}$  to  $65^\circ\text{N}$ ,  $45^\circ\text{W}$  to  $5^\circ\text{E}$ ), which  
234 also coincides with regions of input of Greenland meltwater (47). Recent papers pointed out  
235 relationships between Greenland melting and AMOC variations (48). The spread of FWF values  
236 (0.11 Sv to 0.68 Sv) has been chosen to explore the impact of a large and rapid freshwater  
237 input due to partial melting of the Greenland ice sheet. The highest FWF (0.68 Sv) accounts  
238 for the fact that current climate models are possibly too stable in response to freshwater  
239 release (49). A growing number of modeling results support this assumption by invoking (i)  
240 intrinsic model biases in advection (50–54) and/or in the stratification of the subpolar gyre  
241 (55), (ii) an incorrect representation of freshwater pathways in the absence of an iceberg drift  
242 module (10), or (iii) a too coarse resolution of current ocean models that are not eddy-  
243 resolving (56, 57). All these factors could potentially lead to a limited sensitivity of projected  
244 AMOC to freshwater input. Thus, we analyze here the progressive reduction of the AMOC  
245 corresponding to increased FWF and its potential impacts on the Sahelian region. More  
246 importantly, moderate scenarios (corresponding to 0.11 Sv to 0.34 Sv) have to be considered  
247 regarding the most recent ice sheet observations (e.g., refs. 13, 16, and 58).

### 248 **Statistical method to adjust the IPSL simulated precipitation**

249 The simulated precipitation have been corrected with respect to the WFDEI reanalyses  
250 interpolated to a  $0.5^\circ \times 0.5^\circ$  spatial resolution (34), used as a reference. Here, the “calibration”

251 period covers the 34-year time period 1979-2013, while the “projection” period covers the  
 252 94-year time period 2006-2099.

253 The bias correction method used in this study is a variant of the “Quantile-Mapping” approach  
 254 (e.g., (59, 60)) and allows to account for the climate change signal into the correction (37).  
 255 This method called “Cumulative Distribution Function – transform” (CDF-t) was initially  
 256 developed by (61) and has then been applied in many climate-related studies (e.g., (35–38),  
 257 among others). If  $X$  denotes the random variable representing the modelled variable to be  
 258 corrected, and  $Y$  the random variable representing the reference variable, CDF-t first  
 259 estimates the cumulative distributions  $F_{Yp}$  and  $F_{Xp}$  of the random variables  $Yp$  and  $Xp$  over  
 260 the projection (future) time period before applying a distribution-derived quantile-mapping,  
 261 i.e. trying to map a modelled value  $x_p$  to a value  $y_p$  such that their distributions are equivalent  
 262 (62) :

264

$$263 \quad F_{Yp}(y_p) = F_{Xp}(X_p) \Leftrightarrow y_p = F_{Yp}^{-1}[F_{Xp}(X_p)] \quad (1)$$

265

266 If  $F_{Xp}$  can be directly modelled – parametrically or not – from the data to be corrected in the  
 267 projection period, the modelling of  $F_{Yp}$  is based on the assumption that a mathematical  
 268 transformation  $T$  allows going from  $F_{Xc}$  to  $F_{Yc}$  – the distribution of the random variables  $Yc$   
 269 and  $Xc$  in the calibration period,

$$270 \quad T[F_{Xc}(z)] = F_{Yc}(z) \quad (2)$$

271

272 for any  $z$ , and that  $T$  is still valid in the projection period: that is,

$$273 \quad T[F_{Xp}(z)] = F_{Yp}(z) \quad (3)$$

274

275 Replacing  $z$  by  $F_{Xc}^{-1}(u)$  in eq. (2), where  $u$  is any probability in  $[0, 1]$ , we obtain

$$276 \quad T(u) = F_{Yc}[F_{Xc}^{-1}(u)] \quad (4)$$

277

278 corresponding to a simple definition for  $T$ . Inserting eq. (4) in eq. (3) leads to a modelling of  
 279  $F_{Yp}$ :

$$280 \quad F_{Yp}(z) = F_{Yc} \left[ F_{Xc}^{-1} [ F_{Xp}(z) ] \right] \quad (5)$$

281

282 Once  $F_{Xp}$  and then  $F_{Yp}$  are modelled, a distribution-based quantile-mapping is applied as in  
283 eq. (1). Hence, this CDF-t approach includes the information about the distributions over the  
284 projection time period in the quantile-mapping technique. More details can be found in (37).

285 To refine the bias correction method, a multivariate mapping could be performed, notably to  
286 better account for effect of the meso-scale processes (e.g. AEJ instabilities giving rise to squall  
287 lines) that could counteract those of the large-scale circulation. Such a multivariate approach  
288 would require wind data in altitude that are not currently available. Moreover, multivariate  
289 statistical bias correction methods are only emerging in the literature and are not yet ready  
290 to be used. However, paleoclimatic data reveal that ice-sheet melting produced in the past a  
291 strong decrease of the West African monsoon (3–5) with underlying mechanisms fully similar  
292 to those highlighted in the present study (2), suggesting that the effect of jet instabilities is  
293 insufficient to counterbalance the effect of large-scale circulation (i.e decrease of the  
294 monsoon rainfall).

295

#### 296 **t-test for each simulation**

297 To investigate the significance of the monsoon variations due to the freshwater input, we  
298 use the t-test. We average the total monsoon precipitation on the Sahel area (8°N-18°N;  
299 17°W-15°E) and compare each scenario with the RCP8.5 baseline experiment. The t-test (eq.  
300 6) must be done with stationary series:

$$301 \quad t = \frac{\bar{X}_{scen} - \bar{X}_{rcp85}}{\sqrt{\frac{s_{scen}^2}{n_{scen}} + \frac{s_{rcp85}^2}{n_{rcp85}}}} \quad (6)$$

302

303 where:

304  $t$  is the t-test result

305  $X$  is the sample mean for the scenario under study and the RCP8.5 baseline scenarios

306  $S^2$  is the unbiased estimator of the variance of the two samples

307  $n$  is the number simulated precipitation value in each scenario (i.e 10 for the RCP8.5

308 baseline experiment and 10 for each GrIS scenario)

309 However our scenarios are used in transient experiments. To circumvent this problem, we  
310 calculate the t-test values 10 years by 10 years with a time lag of 1 year (i.e. 2006-2015, 2007-

311 2016,...) to obtain 84 pseudo-stationarity periods by subsampling. We obtain a t-value for each  
312 year between 2011 and 2094. For each t-test we have, 10 values for one GrIS scenario and 10  
313 for the RCP8.5 one, leading to 18 degrees of freedom allowing to have a robust test. A longer  
314 period would lead to non-stationarity of our time series and a shorter period to a test with a  
315 too large variability, and therefore not usable. Using a probability threshold of 97.5%  
316 combined with these 18 degrees of freedom, the critical value is 2.101.

317

### 318 **Water demand of crops**

319 The threshold of crop water demand evolves with time as a function of temperature: the crops  
320 need more water when the temperature increases. The water demand of sorghum cultivation  
321 can be obtained for each model grid point in the Sahel area (8°N-18°N; 17°W-15°E). It is  
322 estimated with the evapotranspiration (ET<sub>0</sub>) given by the Blaney-Criddle technique (63) (eq.  
323 7) with a correction factor *kc*, as suggested by the FAO eq. 8 (64), that accounts for specific  
324 characteristics of a given crop specie:

$$325 \quad ET_{crop} = kc \times A \quad (7)$$

$$326 \quad ET_0 = p (0.46 T_{mean} + 8) \quad (8)$$

327

328 where:

329 *ET<sub>0</sub>* is the potential evapotranspiration (mm/day)

330 *ET<sub>crop</sub>* is the water demand for crop (mm/growing period)

331 *T<sub>mean</sub>* = mean temperature over the monsoon period (° C)

332 *A* is the crop growing period duration (i.e 120 days for sorghum, 105 for millet)

333 *p* = percentage of daytime duration.

334 *kc* = crop factor: 0.78 for sorghum, 0.79 for millet

335

336

### 337 **Surface area and population impacted by rainfall changes**

338 To estimate the variations of the agricultural area due to rainfall changes and the number of  
339 inhabitants impacted by the weakening of precipitation, we computed the land surface area  
340 receiving an amount of precipitation below the required precipitation threshold for sorghum  
341 cultivations. Since the number of inhabitants is given by a 0.5°x0.5° spatial resolution dataset,

342 provided by the Potsdam Institute for Climate Impact Research from a preliminary version of  
343 the SSP population data (the 2012-05-11 data in the IIASA database), the rainfall has been bi-  
344 linearly interpolated on a 0.5°x0.5° grid. For each scenario (RCP 8.5 and GrIS), the area  
345 impacted by rainfall change ( $R(t)$ ) in the Sahel area (8°N-18°N; 17°W-15°E) is obtained year by  
346 year with the following equation:

$$347 \quad R(t) = \sum R_{scen}(t) - \sum R_{ref} \quad (9)$$

348

349 where:

350  $R_{scen}(t)$  represents the area covered by the grid points where the precipitation volume  
351 is above the water demand of crops

352  $R_{ref}$  represents the area covered by the grid points where the precipitation averaged  
353 over the last thirty-year climatic period (1976-2005) is above the water demand of crops.

354

355 To estimate the evolution of the cultivable area affected by a precipitation deficit we express  
356 the number of corresponding pixels in km<sup>2</sup>. When the number of pixels is negative (positive),  
357 the area available for agriculture is smaller (larger) than that of the 1976-2005 climatic period.  
358 The number of inhabitants impacted by rainfall changes is estimated by summing the number  
359 of people living in the corresponding surface area. To count only the rural population with  
360 only rainfed agriculture practices, the surface area where the current population density is  
361 above 200 inhabitants/km<sup>2</sup> is excluded. A positive (negative) value means that a greater  
362 (smaller) number of people is affected by rainfall changes compared to the reference period  
363 (1976-2005).

#### 364 **Code and data availability**

365 All data generated in this study by the IPSLCM5A-LR model for the Greenland scenarios as well  
366 as and the Ferret and Python scripts produced for their analysis are available from the  
367 corresponding author. Other results supporting this study are based on CMIP5 model, WFDEI  
368 Re-analysis data and populations projection, which are available  
369 respectively from [http://cmip-pcmdi.llnl.gov/cmip5/data\\_portal.html](http://cmip-pcmdi.llnl.gov/cmip5/data_portal.html),  
370 [http://www.eu-watch.org/data\\_availability](http://www.eu-watch.org/data_availability) and [http://clima-dods.ictp.it/Users/fcolon\\_g/ISI-](http://clima-dods.ictp.it/Users/fcolon_g/ISI-MIP/)  
371 [MIP/](http://clima-dods.ictp.it/Users/fcolon_g/ISI-MIP/).

372 **Acknowledgements**

373 We thank Michel Crucifix and an anonymous reviewer for their constructive comments  
374 and suggestions that helped improve the manuscript, as well as Serge Janicot and Juliette  
375 Mignot for fruitful discussions. We are also very grateful to Sarah Amram, Jean-Yves  
376 Peterschmitt, and Aurélien Quiquet for technical support, and to Sandra Bouneau and  
377 Sylvain David for numerous exchanges. This work was supported by the French Atomic  
378 Commission (CEA) within the framework of the Variations Abruptes du Climat:  
379 Conséquences et Impacts éNergétiques project funded by the Département des sciences  
380 de la matières (DSM) with the DSM-Energie Program. It benefited from the high  
381 performance computing (HPC) resources made available by Grand Equipement National  
382 de Calcul Intensif, CEA, and Centre National de la Recherche Scientifique. The authors  
383 thank the Potsdam Institute for Climate Impact Research for providing the gridded data  
384 population (SSP3) based on a preliminary version of the SSP population data (the 2012-  
385 05-11 data in the IIASA database). This database has been elaborated within the Inter-  
386 Sectoral Impact Model Intercomparison Project.

387

388 **References**

- 389 1. Hulme M, Doherty R, Ngara T, New M, Lister D (2001) African climate change: 1900-2100. *Clim*  
390 *Res* 17(2):145–168.
- 391 2. Mulitza S, et al. (2008) Sahel megadroughts triggered by glacial slowdowns of Atlantic  
392 meridional overturning. *Paleoceanography* 23(4):PA4206.
- 393 3. Stager JC, Ryves DB, Chase BM, Pausata FSR (2011) Catastrophic drought in the Afro-Asian  
394 monsoon region during Heinrich event 1. *Science* 331(6022):1299–302.
- 395 4. Itambi AC, Dobeneck T Von, Mulitza S, Bickert T, Heslop D (2009) Millennial-scale northwest  
396 African droughts related to Heinrich events and Dansgaard-Oeschger cycles : Evidence in  
397 marine sediments from offshore Senegal. 24:1–16.
- 398 5. Tjallingii R, et al. (2008) Coherent high- and low-latitude control of the northwest African  
399 hydrological balance. *Nat Geosci* 1(10):670–675.
- 400 6. Broecker W, Bond G, Klas M, Clark E, McManus J (1992) Origin of the northern Atlantic's  
401 Heinrich events. *Clim Dyn* 6(3-4):265–273.
- 402 7. Alvarez-Solas J, Robinson A, Montoya M, Ritz C (2013) Iceberg discharges of the last glacial  
403 period driven by oceanic circulation changes. *Proc Natl Acad Sci* 110 (41 ):16350–16354.
- 404 8. Kageyama M, Mignot J (2009) Glacial climate sensitivity to different states of the Atlantic  
405 Meridional Overturning Circulation: results from the IPSL model. *Clim Past* 5(3):551–570.
- 406 9. Swingedouw D, et al. (2009) Impact of Freshwater Release in the North Atlantic under  
407 Different Climate Conditions in an OAGCM. *J Clim* 22(23):6377–6403.
- 408 10. Swingedouw D, et al. (2013) Decadal fingerprints of freshwater discharge around Greenland in  
409 a multi-model ensemble. *Clim Dyn* 41(3-4):695–720.
- 410 11. Church JA, et al. (2013) Sea Level Change. *Climate Change 2013: The Physical Science Basis.*  
411 *Contribution of Working Group I to the Fifth Assessment Report of the Intergovernmental*  
412 *Panel on Climate Change [Stocker, T.F., D. Qin, G.-K. Plattner, M. Tignor, S.K. Allen, J.*  
413 *Boschung, A. Nauels, Y. Xia, pp 1137–1216. Cambridge .*
- 414 12. Straneo F, et al. (2013) Challenges to Understanding the Dynamic Response of Greenland's  
415 Marine Terminating Glaciers to Oceanic and Atmospheric Forcing. *Bull Am Meteorol Soc*

- 416 94(8):1131–1144.
- 417 13. Rignot E, Fenty I, Xu Y, Cai C, Kemp C (2015) Undercutting of marine-terminating glaciers in  
418 West Greenland. *Geophys Res Lett* 42(14):5909–5917.
- 419 14. Gillet-Chaulet F, et al. (2012) Greenland ice sheet contribution to sea-level rise from a new-  
420 generation ice-sheet model. *Cryosph* 6(6):1561–1576.
- 421 15. Paolo FS, Fricker HA, Padman L (2015) Volume loss from Antarctic ice shelves is accelerating.  
422 *Science* 348(6232):327–332.
- 423 16. Mouginot J, et al. (2015) Fast retreat of Zachariæ Isstrøm , northeast Greenland. *Science*  
424 350(6266):1357–1361.
- 425 17. Alvarez-Solas J, Ramstein G (2011) On the triggering mechanism of Heinrich events. *Proc Natl*  
426 *Acad Sci* 108(50):E1359–E1360.
- 427 18. Gomez N, Gregoire LJ, Mitrovica JX, Payne AJ (2015) Laurentide-Cordilleran Ice Sheet saddle  
428 collapse as a contribution to meltwater pulse 1A. *Geophys Res Lett* 42(10):3954–3962.
- 429 19. Dufresne J-L, et al. (2013) Climate change projections using the IPSL-CM5 Earth System Model:  
430 from CMIP3 to CMIP5. *Clim Dyn* 40(9-10):2123–2165.
- 431 20. Manabe S, Stouffer RJ (1988) Two Stable Equilibria of a Coupled Ocean-Atmosphere Model. *J*  
432 *Clim* 1(9):841–866.
- 433 21. Vellinga M, Wood RA, Gregory JM (2001) Processes Governing the Recovery of a Perturbed  
434 Thermohaline Circulation in HadCM3. *J Clim* 15:764–780.
- 435 22. Stouffer R, Yin J, Gregory J (2006) Investigating the causes of the response of the  
436 thermohaline circulation to past and future climate changes. *J Clim* 19(8):1365–1387.
- 437 23. Kageyama M, et al. (2013) Climatic impacts of fresh water hosing under last glacial Maximum  
438 conditions: A multi-model study. *Clim Past* 9(2):935–953.
- 439 24. Jackson R, et al. (2015) Global and European climate impacts of a slowdown of the AMOC in a  
440 high resolution GCM. *Clim Dyn*:3299–3316.
- 441 25. Swingedouw D, Braconnot P, Marti O (2006) Sensitivity of the Atlantic Meridional Overturning  
442 Circulation to the melting from northern glaciers in climate change experiments. 33(April):1–  
443 4.
- 444 26. Peterson LC, Haug GH, Hughen KA, Röhl U (2007) Tropical Atlantic During the Last Glacial  
445 Rapid Changes in the Hydrologic Cycle of the Tropical Atlantic During the Last Glacial. *Science*  
446 (80- ). doi:10.1126/science.290.5498.1947.
- 447 27. Leduc G, et al. (2007) Moisture transport across Central America as a positive feedback on  
448 abrupt climatic changes. *Nature* 445(7130):908–11.
- 449 28. Chiang JCH, Bitz CM (2005) Influence of high latitude ice cover on the marine Intertropical  
450 Convergence Zone. *Clim Dyn*. doi:10.1007/s00382-005-0040-5.
- 451 29. Arbuszewski J a., deMenocal PB, Cléroux C, Bradtmiller L, Mix A (2013) Meridional shifts of the  
452 Atlantic intertropical convergence zone since the Last Glacial Maximum. *Nat Geosci*.  
453 doi:10.1038/ngeo1961.
- 454 30. Niedermeyer EM, et al. (2009) Extratropical forcing of Sahel aridity during Heinrich stadials.  
455 *Geophys Res Lett* 36:L20707.
- 456 31. Liu Y, Chiang JCH, Chou C, Patricola CM (2014) Atmospheric teleconnection mechanisms of  
457 extratropical North Atlantic SST influence on Sahel rainfall. *Clim Dyn* 43(9-10):2797–2811.

- 458 32. Ickowicz A, et al. (2012) Crop-Livestock Production Systems in the Sahel - Increasing Resilience  
459 for Adaptation to Climate Change and Preserving Food Security. *Building Resilience for*  
460 *Adaptation to Climate Change in the Agriculture Sector*, pp 261–294.
- 461 33. Christensen JH, et al. (2013) Climate Phenomena and their Relevance for Future Regional  
462 Climate Change. *Climate Change 2013: The Physical Sci - Ence Basis. Contribution of Working*  
463 *Group I to the Fifth Assessment Report of the Intergovernmental Panel on Climate Change*  
464 [*Stocker, T.F., D. Qin, G.-K. Plattner, M. Tignor, S.K. Allen, J. Boschung, A. Nauels, Y. X.*]
- 465 34. Weedon GP, et al. (2014) The WFDEI meteorological forcing data set: WATCH Forcing Data  
466 methodology applied to ERA-Interim reanalysis data. *Water Resour Res* 50(9):7505–7514.
- 467 35. Oettli P, Sultan B, Baron C, Vrac M (2011) Are regional climate models relevant for crop yield  
468 prediction in West Africa? *Environ Res Lett* 6(1):14008.
- 469 36. Colette A, Vautard R, Vrac M (2012) Regional climate downscaling with prior statistical  
470 correction of the global climate forcing. *Geophys Res Lett* 39(13):L13707.
- 471 37. Vrac M, et al. (2012) Dynamical and statistical downscaling of the French Mediterranean  
472 climate: uncertainty assessment. *Nat Hazards Earth Syst Sci* 12(9):2769–2784.
- 473 38. Vigaud N, Vrac M, Caballero Y (2013) Probabilistic downscaling of GCM scenarios over  
474 southern India. *Int J Climatol* 33(5):1248–1263.
- 475 39. Sultan B, et al. (2013) Assessing climate change impacts on sorghum and millet yields in the  
476 Sudanian and Sahelian savannas of West Africa. *Environ Res Lett* 8(1):014040.
- 477 40. KC S, Lutz W (2014) The human core of the shared socioeconomic pathways: Population  
478 scenarios by age, sex and level of education for all countries to 2100. *Glob Environ Chang.*  
479 doi:10.1016/j.gloenvcha.2014.06.004.
- 480 41. O’Neill BC, et al. (2014) A new scenario framework for climate change research: the concept  
481 of shared socioeconomic pathways. *Clim Change* 122(3):387–400.
- 482 42. Juana JS, Kahaka Z, Okurut FN (2013) Farmers’ Perceptions and Adaptations to Climate  
483 Change in Sub-Sahara Africa: A Synthesis of Empirical Studies and Implications for Public  
484 Policy in African Agriculture. *J Agric Sci* 5(4):121–135.
- 485 43. Neumann B, Vafeidis AT, Zimmermann J, Nicholls RJ (2015) Future Coastal Population Growth  
486 and Exposure to Sea-Level Rise and Coastal Flooding - A Global Assessment. *PLoS One*  
487 10(3):e0118571.
- 488 44. Afolayan AA, Adelekan IO (1999) The role of climatic variations on migration and human  
489 health in Africa. *Environmentalist* 18(4):213–218.
- 490 45. Pontee N (2013) Defining coastal squeeze: A discussion. *Ocean Coast Manag* 84:204–207.
- 491 46. McLeman R a., Hunter LM (2010) Migration in the context of vulnerability and adaptation to  
492 climate change: Insights from analogues. *Wiley Interdiscip Rev Clim Chang* 1(3):450–461.
- 493 47. Bamber J, van den Broeke M, Ettema J, Lenaerts J, Rignot E (2012) Recent large increases in  
494 freshwater fluxes from Greenland into the North Atlantic. *Geophys Res Lett* 39(19):L19501.
- 495 48. Rahmstorf S, et al. (2015) Exceptional twentieth-century slowdown in Atlantic Ocean  
496 overturning circulation. *Nat Clim Chang* 5(5):475–480.
- 497 49. Valdes P (2011) Built for stability. *Nat Geosci* 4(7):414–416.
- 498 50. Liu W, Liu Z, Brady EC (2014) Why is the AMOC monostable in coupled general circulation  
499 models? *J Clim* 27(6):2427–2443.



- 500 51. Liu W, Xie S, Liu Z, Zhu J (2017) Overlooked possibility of a collapsed Atlantic Meridional  
501 Overturning Circulation in warming climate. *Sci Adv* 3(January):e1601666.
- 502 52. Deshayes J, et al. (2013) Oceanic hindcast simulations at high resolution suggest that the  
503 Atlantic MOC is bistable. *Geophys Res Lett* 40(12):3069–3073.
- 504 53. Hofmann M, Rahmstorf S (2009) On the stability of the Atlantic meridional overturning  
505 circulation. *Proc Natl Acad Sci U S A* 106(49):20584–20589.
- 506 54. Weber SL, et al. (2006) The modern and glacial overturning circulation in the Atlantic ocean in  
507 PMIP coupled model simulations. *Clim Past Discuss* 2(5):923–949.
- 508 55. Sgubin G, Swingedouw D, Drijfhout SS, Mary Y, Bennabi A (2017) Abrupt cooling over the  
509 North Atlantic in modern climate models. *Nat Commun* 8:14375.
- 510 56. Spence P, Saenko OA, Sijp W, England MH (2013) North Atlantic Climate Response to Lake  
511 Agassiz Drainage at Coarse and Ocean Eddy-Permitting Resolutions. 2651–2667.
- 512 57. Weijer W, Maltrud ME, Hecht MW, Dijkstra HA, Kliphuis MA (2012) Response of the Atlantic  
513 Ocean circulation to Greenland Ice Sheet melting in a strongly-eddy ocean model.  
514 39(May):1–6.
- 515 58. Noël B, et al. (2017) A tipping point in refreezing accelerates mass loss of Greenland’s glaciers  
516 and ice caps. 8:14730.
- 517 59. Déqué M (2007) Frequency of precipitation and temperature extremes over France in an  
518 anthropogenic scenario: Model results and statistical correction according to observed values.  
519 *Glob Planet Change* 57(1):16–26.
- 520 60. Gudmundsson L, Bremnes JB, Haugen JE, Engen-Skaugen T (2012) Technical Note:  
521 Downscaling RCM precipitation to the station scale using statistical transformations—a  
522 comparison of methods. *Hydrol Earth Syst Sci* 16(9):3383–3390.
- 523 61. Michelangeli P, Vrac M, Loukos H (2009) Probabilistic downscaling approaches: Application to  
524 wind cumulative distribution functions. *Geophys Res Lett* 36(11):L11708.
- 525 62. Panofsky HA, Brier GW (1958) *Some applications of statistics to meteorology* (Mineral  
526 Industries Extension Services, College of Mineral Industries, Pennsylvania State University).
- 527 63. Blaney HF, Criddle WD (1965) Determining Water Requirements For Settling Water Disputes.  
528 *Nat Resour J* 4(1938):29–41.
- 529 64. FAO (2016) 2. Water and soil requirements. Available at:  
530 <http://www.fao.org/docrep/u3160e/u3160e04.htm>.
- 531
- 532

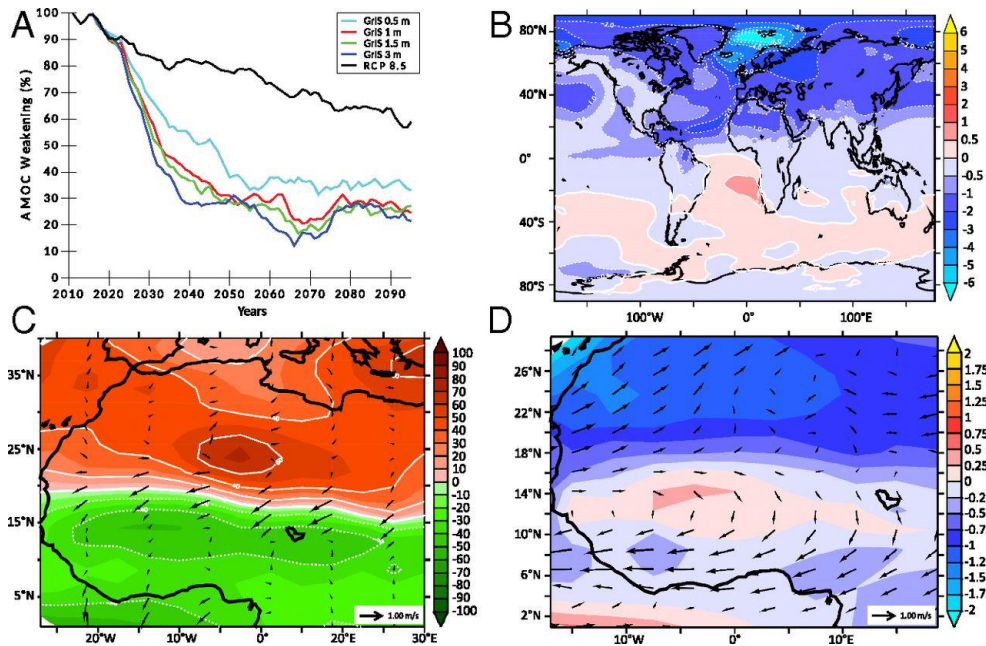


Figure 1: Teleconnection mechanisms linking the Greenland ice sheet melting and the decrease of the Sahelian rainfall. A) AMOC evolution (in % with respect to the present-day values); B) Mean annual temperature anomaly between the 1.5 m GrIS and the RCP8.5 scenarios averaged over the period 2030-2060; C) Same as B) for the sea-level pressure anomaly; and the 10-m winds (black arrows); D) Same as B) for the mean summer (JJAS) temperature anomaly and the 850 hPa winds (black arrows).

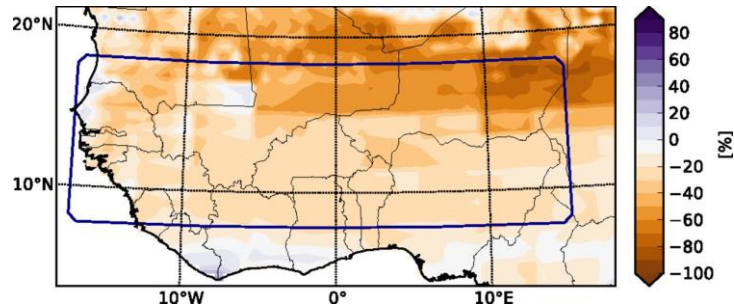


Figure 2: JJAS precipitation anomaly between the 1.5 m GrIS scenario and the RCP 8.5 baseline experiment normalized to the RCP 8.5 values and averaged over 2030-2060. A value of 100 corresponds to a doubling of precipitation and -100 corresponds to zero precipitation. The precipitation values are obtained after applying the statistical method (see Methods). The blue box (8°N-18°N , 17°W-15°E) represents the region under study.

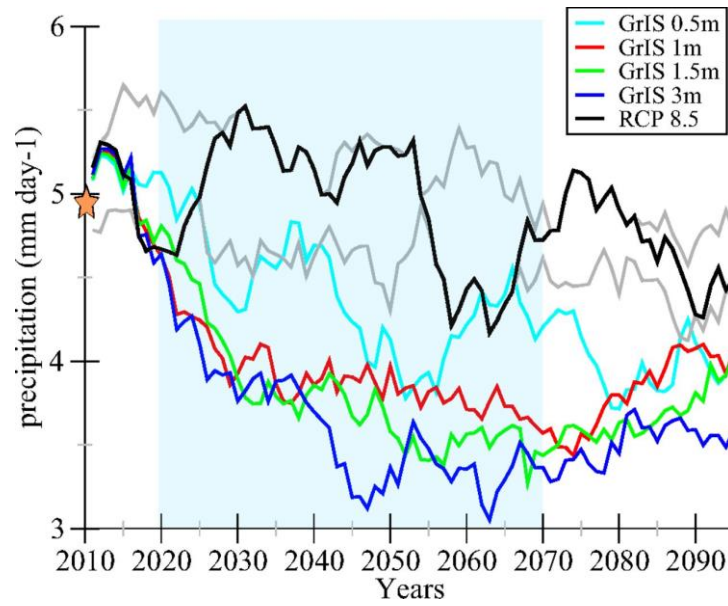
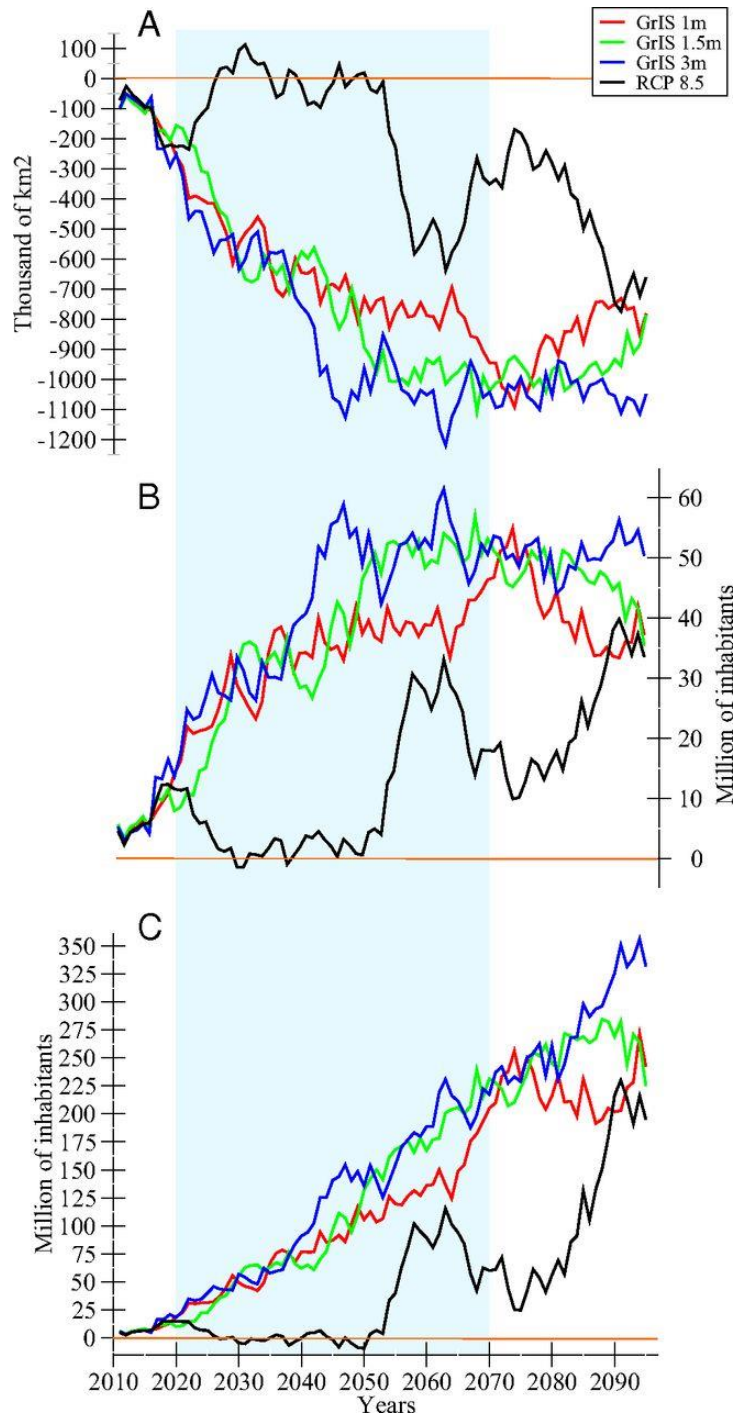


Figure 3: Evolution of JJAS precipitation during the 21<sup>st</sup> century averaged over the Sahel area (8°N-18°N, 17°W-15°E) for the RCP8.5 and the GrIS scenarios. The orange star indicates the simulated JJAS precipitation over the climatic reference period (1976-2005) deduced from the IPSL-CM5A simulated precipitation (4.96 mm). To illustrate the internal model variability, we considered a 4-member dataset of the RCP8.5 scenario, each member differing in initial conditions. The area delimited by the two grey curves represents the range of model variability deduced from the 4-member dataset.



534

Figure 4: Impacts of rainfall change on sorghum cultivation and on population. A) Evolution of the surface area available for sorghum cultivation (i.e. when the average JJAS precipitation is above the sorghum water demand) for each GrIS scenario and for the baseline experiment. The evolution of the available cultivable area is given with respect to the available area averaged over the 1976-2005 reference period deduced from the historical IPSL-CM5A simulated precipitation. Negative (positive) values indicate a loss (gain) of cultivable area; B) Evolution of the number of inhabitants living under the sorghum water demand with respect to the 1976-2005 historical reference period. This evolution is estimated with the assumption that the number of inhabitants is fixed to its 2011 level; C) Evolution of the number of inhabitants living under the sorghum water demand with respect to the 1976-2005 historical reference period. Here, this evolution accounts for the evolution of demography provided by the SSP3 scenario. Both in (B) and (C), positive values indicate that the number of inhabitants living under the sorghum water demand increases with respect to the reference period.